The Phosphorylation State of Threonine-220, a Uniquely Phosphatase-Sensitive Protein Kinase A Site in Microtubule-Associated Protein MAP2c, Regulates Microtubule Binding and Stability†

A. Alexa,‡ G. Schmidt,‡ P. Tompa,‡ S. Ogueta,§ J. Vázquez,§ P. Kulcsár,‡ J. Kovács,|| V. Dombrádi,⊥ and P. Friedrich*,‡

Institute of Enzymology, Biological Research Center, Hungarian Academy of Sciences, Budapest, Hungary, Laboratorio de Química de Proteinas y Proteómica, Centro de Biología Molecular Severo Ochoa, CSICK−Universidad Autónoma de Madrid, Madrid, Spain, Department of Zoology, University of Eötvös Loránd, Budapest, Hungary, and Department of Medical Chemistry, Faculty of Medicine, Medical and Health Science Center, University of Debrecen, Debrecen, Hungary

Received April 3, 2002; Revised Manuscript Received August 5, 2002

ABSTRACT: Phosphorylation of microtubule-associated protein 2 (MAP2) has a profound effect on microtubule stability and organization. In this work a consensus protein kinase A (PKA) phosphorylation site, T^{220}, of juvenile MAP2c is characterized. As confirmed by mass spectrometry, this site can be phosphorylated by PKA but shows less than average reactivity among the 3.5 ± 0.5 phosphate residues incorporated into the protein. In contrast, T^{220} is uniquely sensitive to dephosphorylation: three major Ser/Thr protein phosphatases, in the order of efficiency PP2B > $PP2A_c$ > $PP1_c$, remove this phosphate group first. MAP2c specifically dephosphorylated at this site binds and stabilizes microtubules stronger than either fully phosphorylated or nonphosphorylated MAP2c. Phosphorylation of this site also affects proteolytic sensitivity of MAP2c, which might represent a further level of control in this system. Thus, the phosphorylation state of T^{220} may be a primary determinant of microtubule function.

MAP2[1] is a prominent member of the family of microtubule-binding proteins (including MAP1, MAP2, MAP4, and tau), filamentous proteins that determine the structure and stability of microtubular cytoskeleton (*1*, *2*). It has HMW (a and b) and LMW (c and d) isoforms, produced by alternative splicing. MAP2s have two major structural and functional domains: a C-terminal microtubule-binding domain and an N-terminal projection domain, a large part of which is excised from the LMW variants (*3*). Of the different forms, MAP2b is constitutively expressed throughout life whereas MAP2c is a juvenile form replaced by MAP2a soon after birth except in the olfactory bulb where it persists throughout adulthood (*4*).

The primary function of MAP2, along with other structural MAPs, is to regulate microtubule function via a rather multifarious influence on its stability and dynamics. MAP2 is instrumental in nucleation, polymerization, stability, and bundling (*5*−*7*) but also plays a role in tethering other proteins to microtubules (*8*, *9*), cross-linking microtubules with other cytoskeletal components (*10*, *11*), and controlling microtubular transport (*12*, *13*). To fulfill such a complicated function, the level and pattern of MAP2 phosphorylation is under complex control by various protein kinases and phosphatases (*14*, *15*). Its phosphorylation is spatially and developmentally regulated (*16*−*18*), may reach very high levels (*19*), and undergoes significant changes in developmental or experience-dependent plastic neuronal changes (*17*, *20*−*22*).

The importance of phosphorylation in MAP2 function in cytoskeletal rearrangements is underlined by the fact that MAP2 has a binding site for the regulatory subunit (RII) of PKA (*23*) shared with MAP4 and tau (*8*, *9*); i.e., these MAPs can target kinase action directly to the microtubule network. Further, there is a great deal of direct observations indicating that the level and pattern of MAP2 phosphorylation basically determine the microtubule-binding and stabilizing effect of MAP2 (*24*−*26*). Unfortunately, our knowledge on the contribution of individual protein kinases and phosphatases to the phosphorylation of particular sites and the ensuing cell biological effects is rather limited. So far, the importance of a relatively short segment of MAP2 that includes the

† The work in Hungary was supported by grants T 29059, T 32360, and T 34255 from OTKA, FKFP-0100/2000, and NKFP 1/010. P.T. acknowledges the support of a Bolyai János Scholarship. Work at the CBMSO (S.O. and J.V.) was supported by an institutional research grant from Fundación Ramón Areces and with the support of grant SAF00-0178 from the Dirección General de Enseñanza Superior e Investigación Científica of Spain's Ministry of Education and Culture.

* Corresponding author. Tel: (361) 466-5633. Fax: (361) 466-5465. E-mail: friedric@enzim.hu.

‡ Hungarian Academy of Sciences.

§ CSICK−Universidad Autónoma de Madrid.

|| University of Eötvös Loránd.

⊥ University of Debrecen.

[1] Abbreviations: BA, benzamidine; CBB-R250, Coomassie Brilliant Blue R-250; DTE, dithioerythritol; EGTA, ethylene glycol bis(β-aminoethyl ether)-*N*,*N*,*N*′,*N*′-tetraacetic acid; HMW, high molecular weight; LMW, low molecular weight; MAP2, microtubule-associated protein 2; MES, 2-(*N*-morpholino)ethanesulfonic acid; PIPES, piperazine-*N*,*N*′-bis(2-ethanesulfonic acid); PKA, cAMP-dependent protein kinase; PKC, Ca^{2+}/phospholipid-dependent protein kinase; PMSF, phenylmethanesulfonyl fluoride; $PP1_c$, protein phosphatase 1 catalytic subunit; $PP2A_c$, protein phosphatase 2A catalytic subunit; PP2B, protein phosphatase 2B (calcineurin); PVDF, poly(vinylidene difluoride) membrane; RII, regulatory subunit of PKA; SDS−PAGE, sodium dodecyl sulfate−polyacrylamide gel electrophoresis; Tris, tris(hydroxymethyl)aminomethane.

10.1021/bi025916s CCC: $22.00
Published on Web 09/18/2002

microtubule-binding region and the preceding Pro-rich region of the molecule has been pointed out. Protein kinase C-mediated phosphorylation at several sites (S^{1703}, S^{1711}, and S^{1728}) within the microtubule-binding region has a profound effect on microtubule binding (*25*). Specific phosphorylation at some other, adjacent KXGS motifs (S^{1682} and S^{1713}) by p110 microtubule-affinity regulating kinase (MARK) leads to the dissociation of MAP2 from microtubules and a pronounced increase in the dynamic instability of microtubules (*7*, *27*). MARK phosphorylates homologous sites within MAP4 (*6*, *7*) and tau (*5*); the effect is invariably a stabilization of the microtubule−MAP binding. Similar consequences have been observed for the Pro-rich region nearby (T^{1615}), where specificity of phosphorylation by Pro-directed kinases (MAPK, GSK3, and cdc-2 kinase) (*25*) and of dephosphorylation by PP1 and PP2A has been reported (*28*). Variations in the phosphorylation of these sites are probably central to the physiological control of microtubule function as was seen during brain development (*16*), during synaptic potentiation in hippocampal slices (*22*), and during development in cultured cerebellar granule neurons (*18*). Phosphorylation by the protein kinase directly associated with MAP2, PKA, affects both the microtubule-binding and the Pro-reach regions (*9*) and decreases microtubule binding and nucleating activity (*9*, *12*). Sequence specificity has been mostly studied with tau, showing that PKA phopshorylation is targeted toward both the Pro-rich region (*2*, *4*, *5*) and the KXGS motifs within the microtubule-binding domain (*1*, *5*), with S^{214} of the Pro-rich domain probably being the primary site of phosphate incorporation (*29*). The importance of the latter is emphasized by its prominent phosphorylation during mitosis (*11*) and in Alzheimer's disease (*4*).

The above investigations have almost invariably been performed on HMW MAP2s, and less attention has been paid to the juvenile form, MAP2c, which also plays a role in plastic processes, both before and after birth. Recently, the cell biological effect of PKA phosphorylation of serines within the KXGS motif of each tubulin-binding repeat of MAP2c, corresponding to MARK sites, has been characterized (*30*). It was found that phosphorylation here weakens the MAP2c−microtubule interaction and initiates the translocation of MAP2c to the peripheral actin cytoskeleton (*30*). In the present work we analyzed the specificity of phosphorylation and dephosphorylation of a PKA consensus site within the Pro-rich region of MAP2c at T^{220}. Phosphorylation at this site by PKA affects microtubule binding and stability. Furthermore, this site is uniquely sensitive to protein phosphatases, which makes it a likely candidate for the point of control in various cell biological phenomena, by fast and specific changes in dynamic phosphorylation−dephosphorylation reactions (*21*).

MATERIALS AND METHODS

Materials. Rat MAP2c was expressed in *Escherichia coli* and purified as given in ref *6*. The expression vector was kindly provided by Prof. A. Matus (Friedrich Miescher Institut, Basel, Switzerland). The catalytic subunits of protein phosphatase 1 ($PP1_c$) and 2A ($PP2A_c$) as well as calcineurin (PP2B) were prepared as described earlier (*31*); specific activities were 2350 units/mg for $PP1_c$, 67 units/mg for $PP2A_c$, and 15 units/mg for PP2B. The enzymes were stored in 60% glycerol at −20 °C. Tubulin, prepared according to ref *32*, was kindly provided by Dr. Judit Ovádi (Institute of Enzymology, Biological Research Center, Hungarian Academy of Sciences). Bovine heart PKA RII subunit, prepared according to ref *33* was a gift from Dr. György Vereb (Department of Medical Chemistry, Faculty of Medicine, Medical and Health Science Center, University of Debrecen). [γ-^{32}P]ATP was obtained from IZINTA Ltd. (Budapest, Hungary), and DTE was from Merck. Porcine heart PKA catalytic subunit (catalog no. P8289), endoproteinase Glu-C from *Staphylococcus aureus* V8 (catalog no. P6181), α-chymotrypsin (catalog no. C4129), and all other chemicals were purchased from Sigma Chemical Co.

SDS−PAGE. SDS−PAGE was done according to Laemmli (*34*). The gels were stained with CBB-R250 for visualizing protein bands. After the samples were run on SDS−PAGE, the gel was stained with 0.2% CBB−R250, 50% methanol, and 10% acetic acid, destained with 50% methanol and 10% acetic acid, and washed in several changes of water.

Protein band intensities were determined by densitometry on a Bio-Rad GelDoc 1000 videodensitometer. Optical density was proportional to protein content over the MAP2c concentration range used, as checked in control experiments.

Phosphorylation of MAP2c by PKA. Typically, 0.5 mg/mL MAP2c was phosphorylated by 300 units/mL PKA catalytic subunit in a mixture (100 μL) of 0.1 M PIPES, pH 7.0, 0.5 mM ATP, 1 mM EGTA, 10 mM $MgCl_2$, 5 mM BA, 1 mM PMSF, 1 μM pepstatin, 100 μM leupeptin, 5 μg/mL aprotinin, 2 mM DTE, and 0.4 MBq of [γ-^{32}P]ATP. The mixture was incubated at 37 °C for 60 min if not indicated otherwise. The reaction was stopped by a 2 min boiling. The stoichiometry of phosphate groups incorporated into MAP2c was determined by running the samples on 11% SDS−PAGE, staining the gel with CBB-R250, and measuring radioactivity of the excised MAP2c bands by liquid scintillation counting. To visualize phosphate incorporation, dried SDS gels were exposed to autoradiographic films.

Dephosphorylation of MAP2c by $PP1_c$, $PP2A_c$, and PP2B. Maximally phosphorylated MAP2c (100 μL) was dialyzed for 24 h at 4 °C against three changes (100 mL each) of the appropriate buffer in order to remove radiactive ATP. Ten microliters of the phosphorylated and dialyzed MAP2c (0.5 mg/mL) was dephosphorylated with 6 μL of the enzyme at the given dilution at 31 °C for the time indicated in the following mixtures: 50 mM Tris-HCl, pH 7.5, 1 mM EGTA, and 10 mM DTE ($PP1_c$ and $PP2A_c$) or 50 mM Tris-HCl, pH 7.0, 0.2 mM $CaCl_2$, 10 μM $MnCl_2$, 10 μM calmodulin, and 0.5 mM DTE (PP2B). All mixtures contained 5 mM BA, 0.25 mM PMSF, 1 μM pepstatin, 100 μM leupeptin, and 5 μg/mL aprotinin as protease inhibitors. The reaction was terminated by boiling the samples for 3 min.

Digestion of MAP2c by V8 Protease. Fragmentation of MAP2c by V8 was performed in two ways. In the dephosphorylation reactions, MAP2c samples were treated as above, an aliquot of 4 μL was withdrawn for phosphate determination, and 8 μL (0.1 μg) of V8 protease, diluted in 0.1 M NH_4HCO_3 pH 7.8, was added to the remaining mixtures of 12 μL. The proteolysis was allowed to proceed at 31 °C for 40 min or otherwise for the time indicated. The reaction was terminated by addition of SDS−PAGE sample buffer and boiling the samples for 3 min.

To produce samples for the identification of the phosphorylation site, MAP2c was phosphorylated by PKA as above

except that no radioactive ATP was present. Fifty microliters of the phosphorylation mixture (0.5 mg/mL MAP2c) was digested with 1.4 μg of V8 diluted in 40 μL of 0.1 M NH_4HCO_3, pH 7.8, buffer for 15 min at 31 °C. The reaction was terminated by addition of SDS−PAGE sample buffer and 3 min boiling.

Calpainolytic Cleavage of MAP2c. Proteolysis of nonphosphorylated, maximally phosphorylated, and T^{220}-dephosphorylated MAP2c by calpain was performed at 25 °C in 50 mM Tris-HCl, pH 7.5, 1 mM EGTA, 2 mM $CaCl_2$, 2 mM DTE, 10 mM BA, 2.5 mM PMSF, 0.23 mg/mL MAP2c, and 1 μg/mL calpain. Aliquots were withdrawn at the times indicated, and the reaction was terminated by the addition of SDS−PAGE sample buffer with 5 mM EGTA and boiling the samples for 3 min.

Preparation and N-Terminal Sequencing of the p20 MAP2c Fragment. MAP2c (0.8 mg/mL) was digested for 60 min at 31 °C with 0.02 mg/mL V8 in the following buffer: 0.1 M NH_4HCO_3, pH 7.8, 5 mM BA, 0.25 mM PMSF, and 2 mM DTE. The reaction was stopped by adding SDS−PAGE sample buffer and boiling the mixtures for 2 min. After the sample was run on 11% SDS−PAGE, the digested MAP2c was blotted to PVDF membrane and the p20 protein band was subjected to N-terminal Edman sequencing.

Mass Spectrometry Analysis. The phosphorylated p20 band was resolved by SDS−PAGE, Coomassie Blue-stained, excised, and subjected to in situ digestion with trypsin as described (*35*). A small aliquot (0.5 μL) of the extract was taken up and analyzed by matrix-assisted laser desorption ionization/time of flight (MALDI-TOF) using a Kompact Probe instrument (Kratos-Shimazdu, Manchester, U.K.), equipped with an extended flight tube of 1.7 m and delayed extraction, operating in linear mode, as described previously (*36*). The fractions (0.5 μL) to be analyzed were applied onto target and dried out. Saturated α-cyano-4-hydroxycinnamic acid matrix (0.5 μL) in water−acetonitrile (1:1) containing 0.1% TFA was then added and dried out. Calibration was made externally by using a set of synthetic peptides.

Alkaline phosphatase (AP) treatments were performed by mixing 0.5 μL of peptide extracts with 1 μL of 0.05 unit/μL solution of AP (Roche) and incubating for 15 min at 37 °C; the solution was then deposited onto target and allowed to air-dry before application of the matrix as described above.

Analysis by ion trap mass spectrometry was performed as follows: gel extracts were pooled, dried down, resuspended in 10 μL of 0.5% acetic acid, and subjected to μRP-HPLC separation with on-line analysis by electrospray−ion trap mass spectrometry (LC-ESI−IT MS). A 300 μm i.d. Vydac C18 microcolumn was used at a flow rate of 5 μL/min using a Beckman Gold HPLC instrument equipped with an LCPackings Accurate flow splitter and working at about 0.1 mL/min. The ion trap mass spectrometer, model LCQ (ThermoFinnigan, San Jose, CA), was programmed to work continuously in the "double-play" mode; that is, a MS scan was made to determine whether peaks are present with an intensity above a predefined umbra, in which case a second MS/MS scan is performed on these peaks, using the "dynamic exclusion" method; only two consecutive MS/MS scans are allowed per ion, to achieve the widest sequence coverage. Alternatively, the ion trap detector was programed to perform a continuous sequential operation in the MS/MS mode on the doubly and triply charged ions corresponding to the tentative tryptic phosphopeptide previously determined by MALDI-TOF.

Binding of MAP2c to Microtubules. Microtubules were prepared by tubulin polymerization as follows. Tubulin was dialyzed for 3 h at 4 °C against 50 mM MES, pH 6.2, 5 mM BA, 0.25 mM PMSF, and 2 mM DTE, cleared by a 20 min× 54000 rpm centrifugation at 4 °C, and diluted into 0.1 M PIPES, pH 6.8, 1 mM EGTA, 1 mM $MgCl_2$, 5 mM BA, 1 mM PMSF, and 2 mM DTE polymerization buffer at a final concentration of 1.6 mg/mL. Microtubule polymerization was started by the addition of 20 μM taxol and 1 mM GTP and was allowed to proceed for 15 min at 37 °C. Microtubule assembly was monitored by the increase in absorbance at 350 nm in a Jasco V-550 spectrophotometer equipped with a thermostated cuvette holder.

MAP2c in various phosphorylation states (nonphosphorylated, maximally phosphorylated, and T^{220}-dephosphorylated) was mixed to taxol-stabilized microtubules in polymerization buffer plus 1 mM GTP and 20 μM taxol, at 1.2 mg/mL tubulin and 0.067 mg/mL MAP2c. Binding was allowed at 37 °C for 10 min, and then NaCl at final concentrations ranging from 0 to 200 mM was added to 20 μL aliquots. The samples were incubated for 10 min at 37 °C and centrifuged for 20 min at 54000 rpm at 37 °C. The pellets were suspended with SDS−PAGE sample buffer, boiled for 2 min, run on 11% SDS−PAGE, and stained with CBB-R250. MAP2c and tubulin band intensities were determined by densitometry.

Electron Microscopy. The samples of microtubules prepared with or without addition of MAP2c in various phosphorylation states were sedimented at 54000 rpm, and the pellets were fixed for 1 h in a solution of 2% glutaraldehyde, 0.1% tannic acid, and 0.1 M sodium cacodylate, postfixed in 0.5% OsO_4, and embedded in Durcupan (Fluka). Thin sections were contrasted with uranyl acetate and lead citrate and examined in a JEOL CX 100 electron microscope.

RESULTS

Phosphorylation of MAP2c by PKA. Under our reaction conditions, "in vitro" PKA-mediated phosphorylation resulted in the incorporation of 3.5 ± 0.5 phosphates/MAP2c (Figure 1). Following the prediction by Kenelly and Krebs (*37*) for the PKA substrate consensus sequences, MAP2c appears to contain three major PKA phosphorylation sites (Figure 2), all within the C-terminal microtubule-binding domain. Our results suggest that the three major consensus sites are fully occupied and some additional minor sites are partially phosphorylated.

To identify the sites actually phosphorylated by PKA, we digested the phosphorylated MAP2c with V8 and searched for fragments carrying radioactive phosphate groups. As seen in Figure 1A, V8 digestion resulted in several radiolabeled bands. It should be noted that an apparently paradoxical band corresponding to intact MAP2c appeared only in the 60 min phosphorylated sample. This is probably due to the fact that extensive phosphorylation is unfavorable for V8 digestion in a manner that leaves a small amount of MAP2c uncleaved. This explanation is supported by our finding (not shown) that a protein band by Coomassie staining likewise only appeared at the intact MAP2c position after 60 min phos-

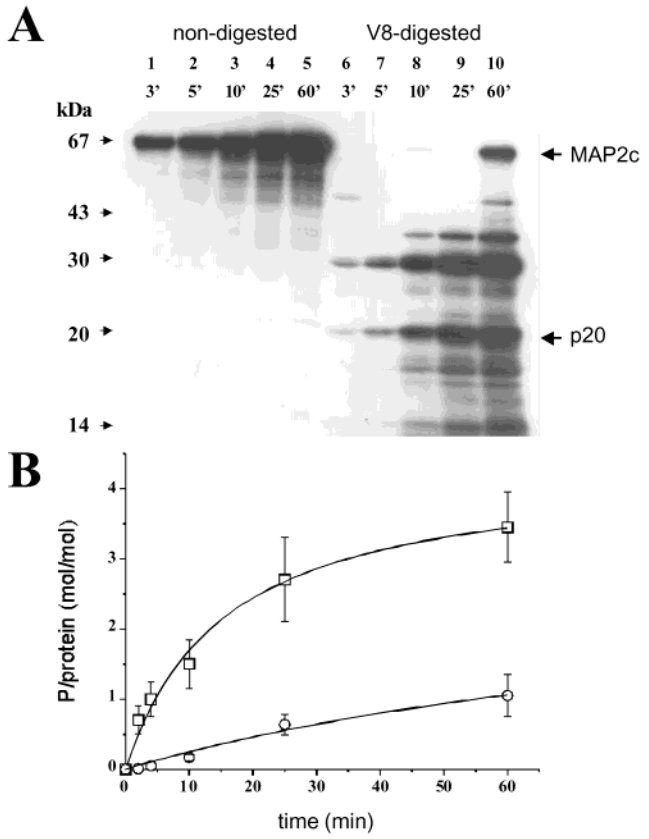

FIGURE 1: Time course of MAP2c phosphorylation by PKA. (A) MAP2c was phosphorylated by PKA for the times indicated and used without further treatment (lanes 1−5) or digested by V8 for 40 min (lanes 6−10) as described in Materials and Methods. The samples run on 11% SDS−PAGE were exposed to autoradiography. (B) Evaluation of the above autoradiogram. Protein/peptide bands were excised from the SDS gels, and their radioactivity was measured using liquid scintillation counting. The data corresponding to the phosphate incorporation into MAP2c (□) and p20 (○) are the mean ± SEM of three independent measurements. The curves fitted to the data points yield an apparent rate constant of 0.065 ± 0.01 min^{-1} for MAP2c and 0.012 ± 0.005 min^{-1} for p20.

phorylation. One of the major phosphorylated polypeptides produced by V8 digestion had a molecular mass of 20 kDa ("p20"). This band is the dominant fragment produced upon prolonged digestion, remaining stable at various V8 concentrations and digestion times (not shown). p20 has the N-terminal sequence of NSFSL, as determined by automated Edman sequencing. The sequence of nine internal peptides from p20 was also determined by HPLC−IT MS/MS analysis; these peptides covered about 50% of the expected p20 sequence (Figure 2). The sequence of the p20 tryptic peptide closest to the C-terminus of MAP2c was VKIE; since trypsin was used for fragmentation, and only this peptide has no basic amino acid in the C-terminal position, it probably corresponds to the C-terminal end of p20. Besides, the acidic nature of the last amino acid of this peptide correlates with the specificity of V8 digestion. p20 was found to contain 1.0 ± 0.2 mol of phosphate/mol in the fully phosphorylated MAP2c form. Analysis of the p20 sequence yielded only one consensus site of phosphorylation, located in T^{220} (see below). We tested whether this p20 phosphorylation site has a preferential reactivity toward PKA. The kinetics of the phosphorylation reactions shows that p20 phosphorylation is about 5-fold slower than that of other sites on MAP2c (Figure 1B). The first phosphate group, therefore, is incorporated by PKA into MAP2c at other sites.

Preferential phosphorylation by PKA might ensue from targeting the kinase to MAP2c via its regulatory subunit. To check this possibility, the above phosphorylation experiment was modified by preincubating MAP2c with PKA RII subunit in a molar ratio of 1:2 to allow formation of the MAP2c−PKA complex prior to starting the reaction with cAMP (50 μM) and ATP. No major difference in the phosphorylation pattern was seen (data not shown); however, the phosphorylation reaction was slightly faster in the case of the PKA holoenzyme.

Phosphorylation Site Analysis. With the aim of determining the exact location of the site of phosphorylation, phosphorylated p20 was separated electrophoretically and subjected to in-gel digestion with trypsin, followed by MALDI-TOF MS analysis of the peptide extract. As shown in Figure 3A, several peptide peaks were observed, corresponding to some of the expected tryptic fragments of p20. One of the peaks had an average mass of 1351.9 Da, which was in good agreement with that of the phosphorylated form of peptide RTTRSEPIRR, containing the T^{220} consensus site. When the peptide extract from p20 was subjected to alkaline phosphatase dephosphorylation, the mass of this peptide was shifted to 1271.9 Da, while the other peptides remained unaffected. The loss of 80 Da indicated that this peptide was phosphorylated. The 80 Da shift could only be detected in the 1351.9 Da peptide, and no traces of the nonphosphorylated form of RTTRSEPIRR were found in the mass map from the raw peptide extract. In addition, other putative phosphorylation sites, such as that at $IGS^{319}T$, were located in peptides which were identified in the nonphosphorylated form (see Figure 2). Taking into account that p20 phosphorylation is of 1:1 stoichiometry, these findings indicate that peptide RTTRSEPIRR was the only one from p20 which was phosphorylated.

To identify the location of the phosphorylated residue in this peptide, we performed a desalting step followed by a direct off-line analysis of the p20 peptide extract by nanospray−ion trap mass spectrometry (not shown). We were unable to detect the presence of any peptide corresponding to the mass determined by MALDI-TOF analysis. Similar negative results were obtained when the peptide extract was directly analyzed by HPLC on line with ion trap mass spectrometry detection (not shown), indicating that this peptide, if present, had a low electrospray ionization efficiency. To circumvent this problem, we turned to a more sensitive technique based on the HPLC−ion trap setup; we took advantage of the high signal-to-noise ratio produced by the ion trap in the MS/MS mode and focused the detector to the exclusive analysis of the expected triply and doubly charged ions corresponding to the tentative phosphopeptide. As shown in Figure 3C, a clear increase in signal was detected at a retention time of 10.26 and 10.30 min, respectively, suggesting that at this time the phosphopeptide was being eluted from the column. The MS/MS spectra obtained for the doubly (not shown) and triply charged ion (Figure 3D) were dominated by the loss of phosphate (98 Da, indicated by a Δ symbol), as expected for a Thr-phosphorylated peptide. Analysis of the MS/MS spectrum from the triply charged ion allowed us to locate the phosphorylated residue in the third amino acid position, as

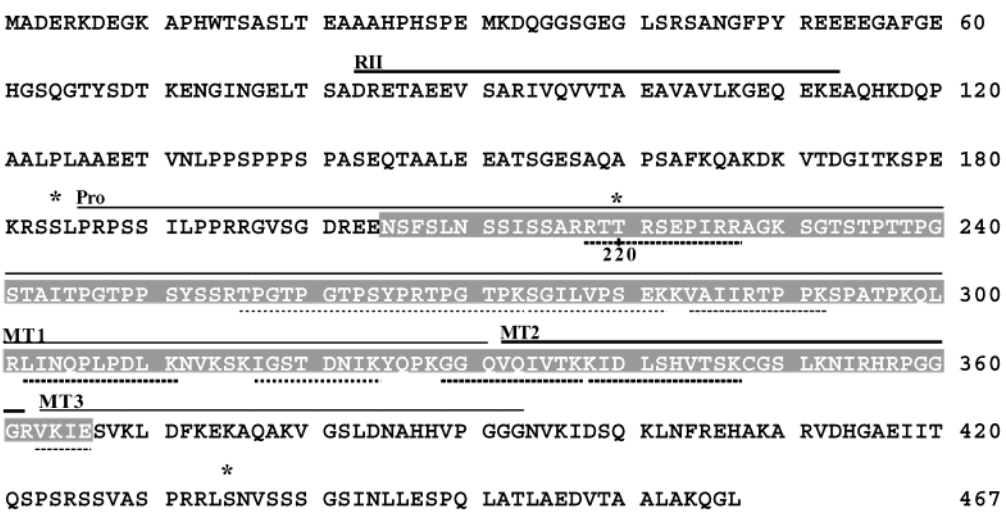

FIGURE 2: Scheme of MAP2c sequence. The sequence of rat MAP2c is shown with the consensus PKA phosphorylation sites marked by asterisks. Functionally or structurally important regions, such as the PKA regulatory subunit binding site (RII), the proline-rich (Pro) segment, and three microtubule-binding domains (MT1, MT2, and MT3), are shown by an overscore. The sequence which corresponds to p20 is shaded in gray. Tryptic internal fragments of p20 identified by HPLC−IT MS/MS are underscored by dotted lines.

deduced from the presence of the y_8/y_7 and b_2/b_3 ion pairs. This modified Thr residue corresponded to T[220].

Site-Specific Dephosphorylation of MAP2c. Dephosphorylation was studied with the major Ser/Thr protein phosphatases, $PP1_c$, $PP2A_c$, and PP2B. MAP2c maximally phosphorylated by PKA was treated with either of the phosphatases and digested by V8 protease. As shown in Figure 4A for $PP1_c$, the p20 site is uniquely sensitive to dephosphorylation: p20 is dephosphorylated before whole MAP2c is much affected. Figure 4B shows that under conditions when the phosphatase removes one phosphate equivalent from fully phosphorylated MAP2c, p20 gets almost completely dephosphorylated; the same results were obtained with the other two phosphatases. This observation indicates that the phosphate group on T[220] is probably quite mobile, being subject to a much faster turnover than any other PKA site in MAP2c.

To compare the phosphatases in terms of effectiveness toward the p20 site, MAP2c was dephosphorylated by each of the three phosphatases at both 37 and 570 microunit/mL activities, digested by V8, and processed as in the previous section. At 37 microunits/mL, the p20 site was only dephosphorylated by PP2B and was left virtually unaffected by the other two enzymes (Figure 5A). At 570 microunits/mL, the p20 site was also fully dephosphorylated by PP2A (Figure 5B). These two experiments show that calcineurin is the most effective, followed by PP2A; the least effective of the three is PP1. Nevertheless, all three phosphatases show a high preference toward the p20 site.

Effect of T[220] Dephosphorylation on Microtubule Binding and Stability. Changes in the level and pattern of MAP2 phosphorylation have a profound effect on microtubule binding of the molecule (see the introduction). Phosphorylation might be particularly critical in the Pro-rich region just preceding the tubulin-binding repeat (*29*), exactly where T[220] is located. To address this issue, microtubule binding of MAP2c in various phosphorylation states was measured. Figure 6A shows that salt-dependent dissociation of MAP2c from taxol-stabilized microtubules is promoted by maximal PKA phosphorylation: at the physiological ionic strength of 150 mM NaCl, MAP2c bound to the microtubules under the given conditions decreases from 35% to 25% of that bound under lower ionic strength conditions. More importantly, the removal of a single phosphate group from the mobile site T[220] not only reverts this effect but enhances the microtubule binding of MAP2c; at physiological ionic strength 60% of MAP2c remains attached to microtubules. As seen in Figure 6B, the phosphorylation status of this single, phosphatase-sensitive site not only affects binding to stabilized microtubules but has a parallel effect on promoting microtubule polymerization as well. Electron microscopic analysis demonstrates the presence of numerous, loosely arranged, intact microtubules in the pellets obtained from these polymerization assays (Figure 6C).

Effect of T[220] Dephosphorylation on Calpain Sensitivity. Phosphorylation by PKA and specific dephosphorylation of T[220] may also influence the proteolytic degradation of the protein, thus providing a further level of control of microtubule−MAP2c interaction. We tested if p20 phosphorylation affects MAP2c proteolysis by μ-calpain, the Ca^{2+}-activated intracellular cysteine protease, by comparing calpainolytic digestion of nonphosphorylated, maximally phosphorylated, and T[220]-dephosphorylated MAP2c (Figure 7). It was found that although the differences are not large, a trend that specifically dephosphorylated MAP2c is less sensitive to cleavage than the maximally phosphorylated and nonphosphorylated forms can be discerned: the apparent first-order rate constants for the three reactions are 0.13 min^{-1} (34%), 0.26 min^{-1} (68%), and 0.38 min^{-1} (100%), respectively.

DISCUSSION

There is ample evidence that MAP2 plays a crucial role in microtubule function via regulating microtubule dynamics and organization. This function of MAP2 is probably under tight control by protein phosphorylation. As MAP2 can be multiply phosphorylated, and is a very good substrate for most protein kinases and phosphatases, its phosphorylation pattern may undergo tremendous variations in vivo. Understanding the cellular readout of these changes requires detailed studies of the relation of MAP2 behavior and phosphorylation. Such studies so far have revealed that

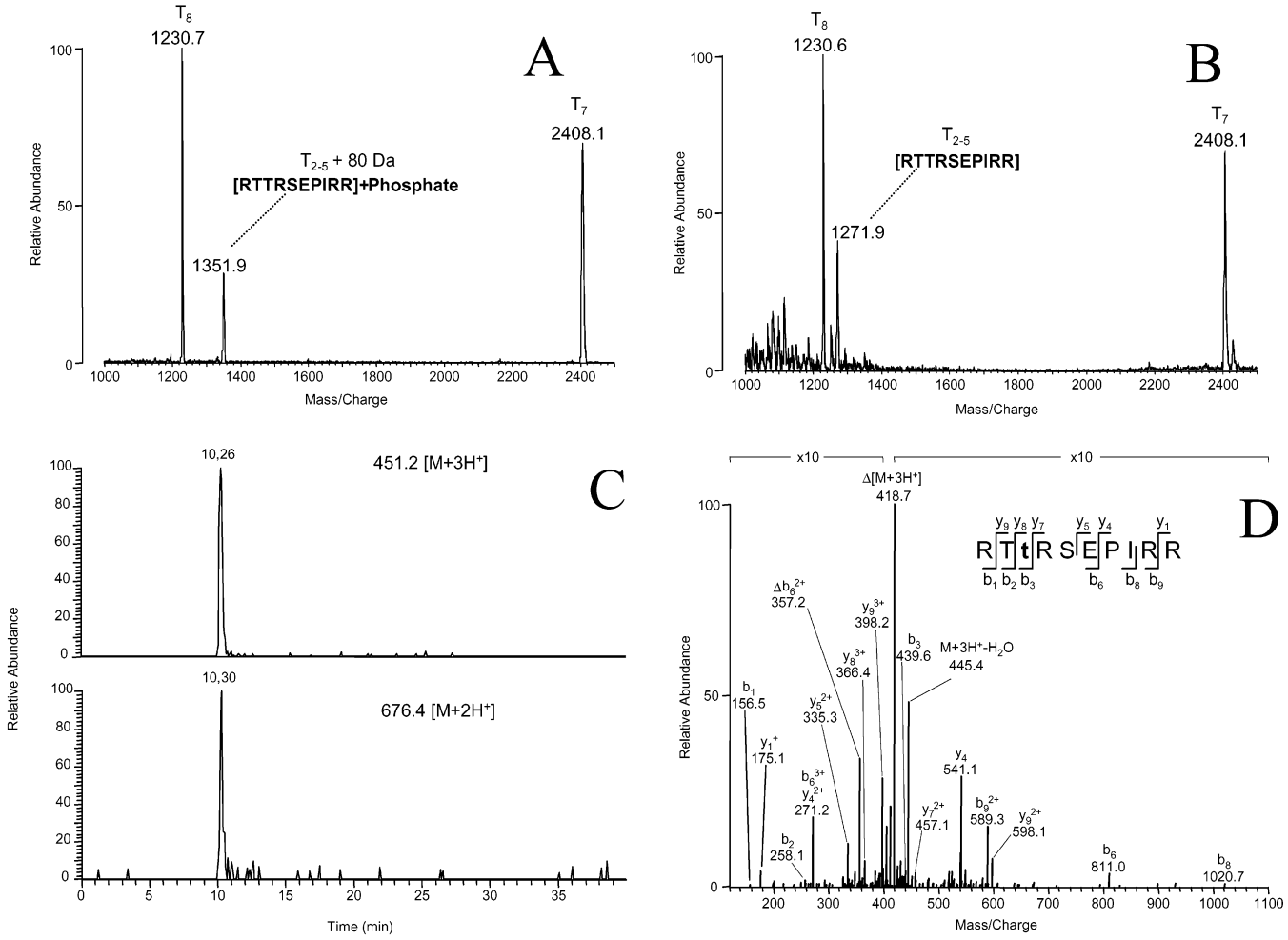

FIGURE 3: Identification of the site of phosphorylation in the p20 MAP2c fragment. (A, B) MALDI-TOF peptide mass maps obtained from in-gel tryptic digestion of p20 before (A) and after (B) incubation with alkaline phosphatase. The identity of the tryptic fragments is indicated by their position in the p20 sequence. The sequence of the tentative phosphopeptide is given inside square brackets. The *m*/*z* values obtained in these experiments correspond to the singly charged peptide ions ($M + H^+$). (C, D) Analysis of the peptide extract from the p20 band by HPLC−electrospray ion trap mass spectrometry. The ion trap detector was focused to perform sequential MS/MS spectra of the ions corresponding to the triply ($M + 3H^+$, *m*/*z* 451.2) and doubly charged ions ($M + 2H^+$, *m*/*z* 676.4) of the tentative phosphopeptide. In (C) the signal obtained by the detector corresponding to the neutral loss of phosphate (32.67 Da for the triply charged and 49 Da for the doubly charged ion) was plotted against the retention time of the HPLC column. In (D) the MS/MS spectrum obtained from the fragmentation of the triply charged peptide ion is shown. The signal was averaged using the spectra acquired around the 10.26 min peak and was background-subtracted using the spectra acquired before and after the peak. The assignment of the fragmentation series was made using the standard nomenclature and was indicated on the tentative phosphopeptide sequence. Ions originating by neutral loss of phosphate from any fragment ions are labeled using the △ prefix. The phosphorylated threonine residue was indicated by a bold, lowercase letter.

phosphorylation by various kinases (PKC, MARK, and Pro-directed kinases) in a relatively short segment of MAP2 has a strong influence on the microtubule-binding and stabilizing capacity of the molecule. Nevertheless, little attention has been payed to the specificity of action of the endogenous kinase of MAP2, i.e., PKA, and of protein phosphatases on MAP2c, the juvenile MAP2 form. This is an alternatively spliced variant of HMW-MAP2 and carries a subset of its phosphorylation sites. Owing to its much smaller size, it is likely to be distinct from HMW MAP2 in its posttranslational regulation and function; at the same time it is beneficially exempt from the almost inextricable complexity of HMW MAP2.

In this work we investigated the PKA-mediated phosphorylation of MAP2c. We found that PKA can incorporate 3.5 ± 0.5 mol of phosphate/mol of MAP2c. Ozer and Halpain (*30*) found a maximum of 3 mol of phosphate/mol of MAP2c incorporation by PKA. After a short incubation time (30 s) they identified three phosphorylation sites, the S^{319}, S^{350}, and S^{382}, among many others. These three sites lie within the KXGS motif of each of the three tubulin-binding repeats and correspond to sites phosphorylated by MARK in MAP2 (*6*) and also in tau (*5*). The effect of Ser-Ala and Ser-Glu mutations of these sites on the MAP2−microtubule interaction provides evidence for their importance within the cell. On the basis of the consensus sequences for PKA, however, these sites are likely to be minor phosphorylation sites only, since at least one arginine at position −2 or −3 is needed for strong phosphorylation (*37*). Furthermore, their two-dimensional phosphopeptide map shows well over three different phosphorylation sites, although the authors selected only three of these for study.

In our investigation, we characterized one of the major phosphorylation sites within the Pro-rich region by means of V8 digestion followed by a detailed analysis by a combination of mass spectrometry techniques. We identified

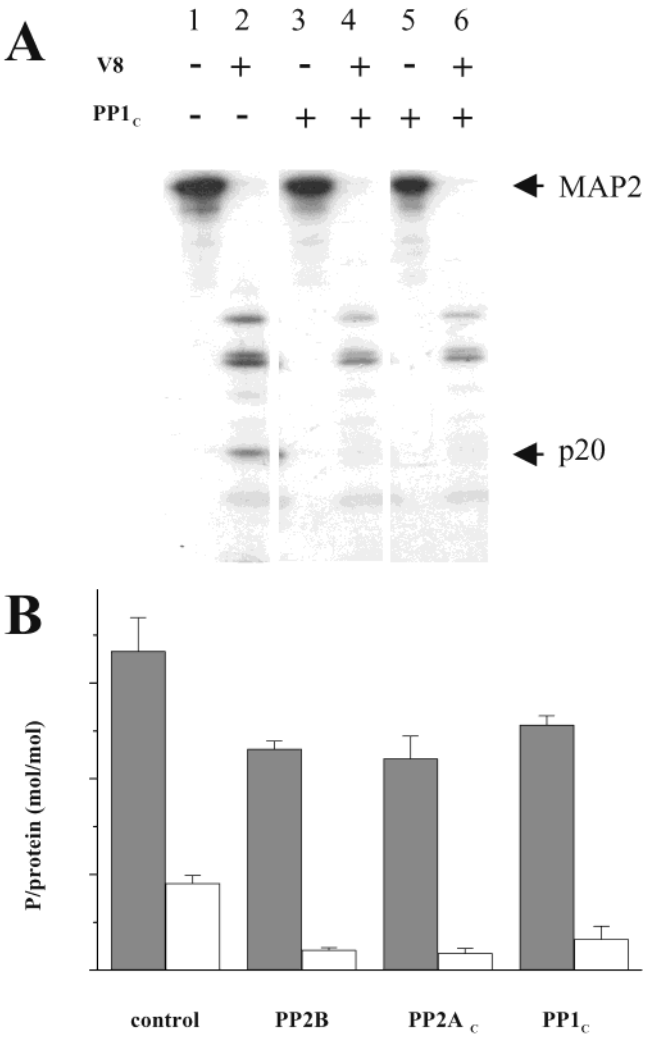

FIGURE 4: Specificity of T^{220} dephosphorylation. (A) MAP2c (0.31 mg/mL), maximally phosphorylated by PKA (lanes 1 and 2), was dephosphorylated by $PP1_c$ (13 milliunits/mL) at 31 °C for 1 min (lanes 3 and 4) and for 5 min (lanes 5 and 6), and the reaction was terminated by boiling the samples for 3 min. Samples were then not treated (lanes 1, 3, and 5) or treated with V8 protease for 24 min (lanes 2, 4, and 6), run on 11% SDS−PAGE, and exposed to autoradiography. Phosphate content of MAP2c and the p20 peptide is shown in the figure. Note that the primary site of dephosphorylation resides in p20. (B) Removal of about one phosphate group from MAP2c (maximally phosphorylated) by any of the phosphatases tested causes almost complete dephosphorylation of p20. MAP2c (0.31 mg/mL) was dephosphorylated for 3 min by PP2B (36.2 microunits/mL), $PP2A_c$ (377.8 microunits/mL), and $PP1_c$ (6.67 milliunits/mL), and the phosphate content of the intact molecule (filled bars) and p20 peptide (open bars) was determined. Values indicate the mean ± SEM for three to six separate measurements.

a region within MAP2c (p20) which was phosphorylated with a 1:1 stoichiometry, and our data indicated that T^{220} was the only phosphorylated residue in this region. This site is distinguished by its unique sensitivity to dephosphorylation, while it is not preferentially phosphorylated by the PKA catalytic subunit: the first phosphate group is incorporated into some other site outside the p20 fragment, possibly within the microtubule-binding region.

When PKA is targeted to MAP2c by its regulatory subunit, all the sites become slightly more reactive, but to the same extent, the phosphorylation of T^{220} is not preferred. Thus, the RII subunit, possibly via PKA anchoring, makes all its phosphorylation sites more susceptible. The importance of

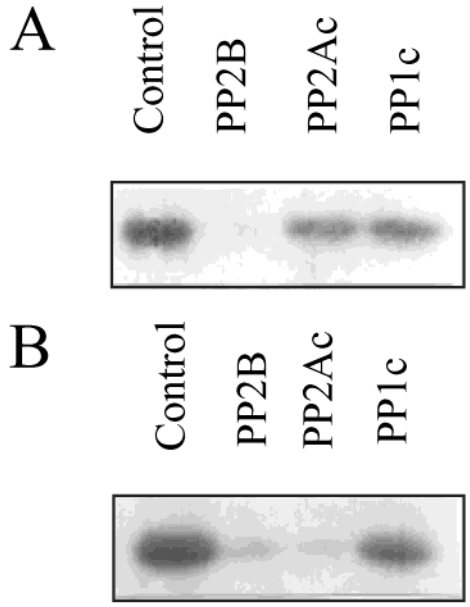

FIGURE 5: Order of effectiveness of PP2B, $PP2A_c$, and $PP1_c$ in T^{220} dephosphorylation. Dephosphorylation of 0.31 mg/mL MAP2c was carried out with all three phosphatases at 31 °C for 10 min; V8-digested samples were run on 11% SDS−PAGE and exposed for autoradiography (only the p20 band is shown). The activity of the phosphatases was uniformly set to 37 microunits/mL (A) or 570 microunits/mL (B) in the mixtures.

T^{220}, nevertheless, is underlined by the observations that microtubule binding and stabilization are particularly sensitive to the phosphorylation status of this site: MAP2c phosphorylated at the other (two) sites, but not at T^{220}, binds and stabilizes microtubules significantly stronger than either nonphosphorylated or fully PKA-phosphorylated MAP2c. This observation raises the possibility of site-specific bidirectional control of MAP2 action and represents a significant deviation from previous one-sided data that show only weakening of microtubule−MAP2 interaction upon phosphorylation by PKA (*5*, *9*, *10*) or by other kinases, such as MARK (*6*, *7*), PKC (*16*), or Pro-directed kinases (*15*) so far. Our result recalls the classical observation that the site of phosphate incorporation, rather than its amount, is critical in determining the microtubule-binding activity of MAP2 (*24*). A further appeal of our observations is that this site is extremely sensitive to phosphatase action as all the major phosphatases tested (in decreasing order of efficiency PP2B, PP2A, and PP1) dephosphorylate it fully before touching the other sites. Thus, because of PKA targeting and phosphatase sensitivity, this site contains a mobile phosphate group that affects control of microtubule function.

Intriguingly, the location and behavior of this T^{220} are similar to Ser^{214} in tau protein, which is also phosphorylated by PKA. This phosphorylation decreases the microtubule-stabilizing and microtubule-nucleating effects exerted by tau (*29*) and is prominent during cell cycle progression (*11*) or in Alzheimer's disease (*4*). This sensitive site may well be equally functional in HMW MAP2. Most studies show the importance of this region in MAP2a/b, and the sequence identity suggests a similar or identical sensitivity of this site. Therefore, this region might serve as a regulator of microtubule binding.

MAP2c phosphorylated on all PKA sites except T^{220} was found to be more resistant to attack by μ-calpain than the

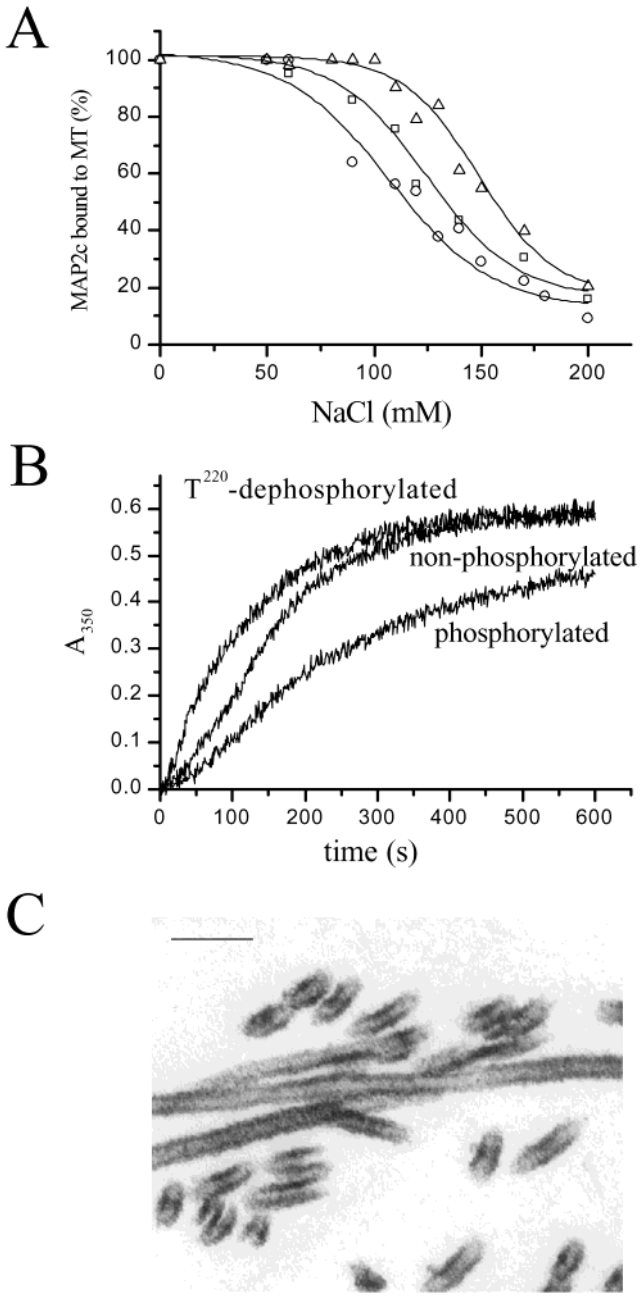

FIGURE 6: Effect of T^{220} dephosphorylation on the microtubule−MAP2c interaction and microtubule polymerization (A) Nonphosphorylated (□), maximally phosphorylated (○), and T^{220}-dephosphorylated (△) MAP2c (0.067 mg/mL) was bound to taxol-stabilized microtubules (1.2 mg/mL) as described in Materials and Methods. NaCl was added to aliquots at different concentrations (0−200 mM), and after 10 min incubation microtubules were centrifuged. MAP2c bound to microtubules was determined by SDS−PAGE and densitometry. Values indicate averages of six separate measurements. (B) MAP2c (nonphosphorylated, maximally phosphorylated, and T^{220}-dephosphorylated) at 0.3 mg/mL was added to 1.6 mg/mL tubulin in the presence of 130 mM NaCl, and the assembly of microtubules was monitored at 37 °C by following absorbance at 350 nm. The tubulin polymerization was carried out in the absence of taxol. (C) Nonphosphorylated MAP2c was added to tubulin as indicated in (B), and the product of polymerization was studied in the electron microscope (see Materials and Methods). The sample contains intact microtubules. Scale bar: 100 nm.

fully PKA-phosphorylated and the nonphosphorylated protein. Earlier work on HMW MAP2 in this laboratory (*38*) and elsewhere (*39*) has shown that phosphorylation by PKA

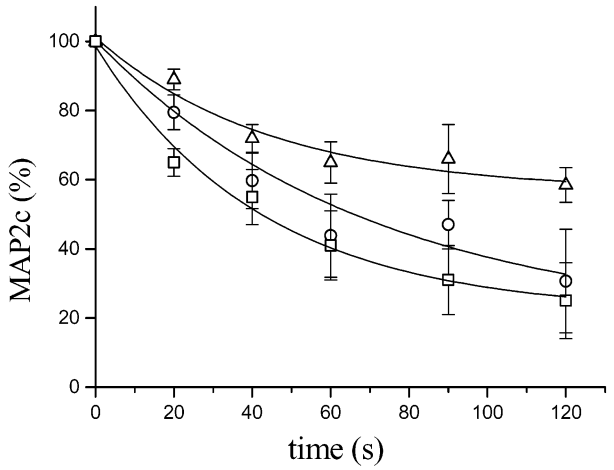

FIGURE 7: Effect of T^{220} dephosphorylation on calpainolytic degradation of MAP2c. Nonphosphorylated (□), maximally phosphorylated (○), and T^{220}-dephosphorylated (△) MAP2c (0.28 mg/mL) was digested by 1 μg/mL μ-calpain for the time indicated, the reaction was terminated, and the remaining intact MAP2c was determined by SDS−PAGE and densitometry. The values indicate the mean ± SEM for three separate experiments.

conferred substantial resistance to the protein against cleavage by calpain. Interestingly, however, calpain sensitivity as a function of the extent of phosphorylation shows a biphasic behavior; i.e., incorporation of the first two to three phosphate groups increases, rather than descreases, susceptibility to calpain (*38*). It remains to be seen whether this transient protection is due to a phosphorylation pattern in which T^{1583} (the residue of HMW MAP2 corresponding to T^{220} in MAP2c) is unphosphorylated. Being colocalized in the dendrites of neurons, MAP2s are likely to be attacked by calpain when the enzyme gets activated during plastic synaptic changes. It is worth to recall here that the Ca^{2+}-activated phosphatase is most efficient in removing the phosphate from T^{220}.

A further interesting issue is the structural impact of the phosphorylation pattern of MAP2c. The fact that T^{220} is not preferentially reactive toward PKA but uniquely sensitive to protein phosphatases points to a structural transition of MAP2c induced by PKA phosphorylation. Native MAP2c has no definite secondary structure, it is a random coil, so each phosphorylation site is equally accessible to the kinase. Phosphorylation endows MAP2c with a definite structure, in which the T^{220} is exposed to protein phosphatases, while other sites are (partially) buried. As a further consequence of this structural transition, it is very likely that the sequence in which MAP2c is phosphorylated by the different kinases plays an important role, similar to the case of tau, where sequential phosphorylation events lead to the formation of the Alzheimer-specific epitope (*40*).

REFERENCES

1. Matus, A. (1994) in *Microtubules* (Hyams, J. S., and Lloyd, V. W., Eds.) pp 155−166, Wiley-Liss, New York.
2. Drewes, G., Ebneth, A., and Mandelkow, E. M. (1998) *Trends Biochem. Sci. 23*, 307−311.
3. Papandrikopoulou, A., Doll, T., Tucker, R. P., Garner, C. C., and Matus, A. (1989) *Nature 340*, 650−652.
4. Viereck, C., Tucker, R. P., and Matus, A. (1989) *J. Neurosci. 9*, 3547−3557.
5. Chen, J., Kanai, Y., Cowan, N. J., and Hirokawa, N. (1992) *Nature 360*, 674−677.

6. Ferralli, J., Doll, T., and Matus, A. (1994) *J. Cell Sci. 107*, 3115−3125.
7. Ludin, B., Ashbridge, K., Funfschilling, U., and Matus, A. (1996) *J. Cell Sci. 109*, 91−99.
8. Scott, J. D., Stofko, R. E., McDonald, J. R., Comer, J. D., Vitalis, E. A., and Mangili, J. A. (1990) *J. Biol. Chem. 265*, 21561−21566.
9. Hausken, Z. E., Dell'Acqua, M. L., Coghlan, V. M., and Scott, J. D. (1996) *J. Biol. Chem. 271*, 29016−29022.
10. Yamauchi, T., and Fujisawa, H. (1988) *Biochim. Biophys. Acta 968*, 77−85.
11. Pedrotti, B., Colombo, R., and Islam, K. (1994) *Biochemistry 33*, 8798−8806.
12. Lopez, L. A., and Sheetz, M. P. (1995) *J. Biol. Chem. 270*, 12511−12517.
13. Sato-Harada, R., Okabe, S., Umeyama, T., Kanai, Y., and Hirokawa, N. (1996) *Cell. Struct. Funct. 21*, 283−295.
14. Friedrich, P., and Aszódi, A. (1991) *FEBS Lett. 295*, 5−9.
15. Avila, J., Dominguez, J., and Diaz-Nido, J. (1994) *Int. J. Dev. Biol. 38*, 13−25.
16. Sanchez, C., Diaz-Nido, J., and Avila, J. (1995) *Biochem. J. 306*, 481−487.
17. Riederer, B. M., Draberova, E., Viklicky, V., and Draber, P. (1995) *J. Histochem. Cytochem. 43*, 1269−1284.
18. Sanchez Martin, C., Diaz-Nido, J., and Avila, J. (1998) *Neuroscience 87*, 861−870.
19. Tsuyama, S., Terayama, Y., and Matsuyama, S. (1987) *J. Biol. Chem. 262*, 10886−10892.
20. Aoki, C., and Siekevitz, P. (1985) *J. Neurosci. 5*, 2465−2483.
21. Quinlan, E. M., and Halpain, S. (1996) *Neuron 16*, 357−368.
22. Sanchez, C., Ulloa, L., Montoro, R. J., Lopez-Barneo, J., and Avila, J. (1997) *Brain Res. 765*, 141−148.
23. Rubino, H. M., Dammerman, M., Shafit-Zagardo, B., and Erlichman, J. (1989) *Neuron 3*, 631−638.
24. Brugg, B., and Matus, A. (1991) *J. Cell Biol. 114*, 735−743.
25. Ainsztein, A. M., and Purich, D. L. (1994) *J. Biol. Chem. 269*, 28465−28471.
26. Itoh, T. J., Hisanaga, S., Hosoi, T., Kishimoto, T., and Hotani, H. (1997) *Biochemistry 36*, 12574−12582.
27. Illenberger, S., Drewes, G., Trinczek, B., Biernat, J., Meyer, H. E., Olmsted, J. B., Mandelkow, E. M., and Mandelkow, E. (1996) *J. Biol. Chem. 271*, 10834−10843.
28. Sanchez, C., Tompa, P., Szűcs, K., Friedrich, P., and Avila, J. (1996) *Eur. J. Biochem. 241*, 765−771.
29. Illenberger, S., Zheng-Fischhofer, Q., Preuss, U., Stamer, K., Baumann, K., Trinczek, B., Biernat, J., Godemann, R., Mandelkow, E. M., and Mandelkow, E. (1998) *Mol. Biol. Cell 9*, 1495−1512.
30. Ozer, R. S., and Halpain, S. (2000) *Mol. Biol. Cell 11*, 3573−3587.
31. Ulloa, L., Dombrádi, V., Diaz-Nido, J., Szűcs, K., Gergely, P., Friedrich, P., and Avila, J. (1993) *FEBS Lett. 330*, 85−89.
32. Na, G. C., and Timasheff, S. N. (1986) *Biochemistry 25*, 6214−6222.
33. Vereb, G., Erdödi, F., Tóth, B., and Bot, G. (1986) *FEBS Lett. 197*, 139−142.
34. Laemmli, U. K. (1970) *Nature 227*, 680−685.
35. Shevchenko, A., Wilm, M., Vorm, O., Jensen, O. N., Podtelejnikov, A. V., Neubauer, G., Mortensen, P., and Mann, M. (1996) *Biochem. Soc. Trans. 24*, 893−896.
36. Garcia, M. A., Campillos, M., Ogueta, S., Valdivieso, F., and Vazquez, J. (2000) *J. Mol. Biol. 301*, 807−816.
37. Kennelly, P. J., and Krebs, E. G. (1991) *J. Biol. Chem. 266*, 15555−15558.
38. Alexa, A., Tompa, P., Baki, A., Vereb, G., and Friedrich, P. (1996) *J. Neurosci. Res. 44*, 438−445.
39. Johnson, G. V., and Foley, V. G. (1993) *J. Neurosci. Res. 34*, 642−647.
40. Zheng-Fischhofer, Q., Biernat, J., Mandelkow, E. M., Illenberger, S., Godemann, R., and Mandelkow, E. (1998) *Eur. J. Biochem. 252*, 542−552.

BI025916S